1997

Semiclassical Model of Λ-doublet States in Diatomic Molecules

Laurie J. Kovalenko

John B. Delos
William & Mary, jbdelos@wm.edu

Recommended Citation

Kovalenko, Laurie J. and Delos, John B., Semiclassical Model of Λ-doublet States in Diatomic Molecules (1997). *Journal of Chemical Physics*, 107(14), 5460-5472.
https://doi.org/10.1063/1.474251

Semiclassical model of Λ-doublet states in diatomic molecules

Laurie J. Kovalenko
Natural Sciences Collegium, Eckerd College, St. Petersburg, Florida 33711

John B. Delos
Physics Department, College of William and Mary, Williamsburg, Virginia 23185

(Received 4 February 1997; accepted 26 June 1997)

An intuitive picture of Λ-doubling in diatomic molecules is presented using a semiclassical theory. A common view of Λ-doubling as arising from electrons ''lagging'' behind the rotating internuclear axis is shown to be misleading; rather, the eigenfunctions are symmetric about the molecular axes and can be expressed as a superposition of pure nonrotating orbitals and travelling waves. These results are shown to be consistent with a full quantum treatment. We also examine, for the first time, time-dependent states, by monitoring expectation values of electronic- and nuclear-angular momenta. For low rotation frequency, the expectation value of the electronic-angular momentum locks onto the rotating internuclear axis, while for high rotation frequency it locks onto the space-fixed total-angular momentum axis. At intermediate frequencies is a complicated behavior.
 [S0021-9606(97)01937-5]

I. INTRODUCTION

The phenomenon of Λ-doubling has been known for a long time and has been successfully treated theoretically in the early 20th century by several of the Old Masters.[1–3] More recent full quantum treatments include those by Hougen,[4] Zare *et al.*,[5] and Helm *et al.*[6] However, a physical picture of Λ-doubling using an intuitive semiclassical model is lacking.

Since typical energy splittings are less than $1\ \mathrm{cm}^{-1}$, Λ-doubling may appear to be justifiably negligible. Even for states differing by such a negligible amount of energy, though, there is a big difference between them in terms of the spatial orientation of their charge distribution. Preferential population of one component over another has been seen in numerous cases including collisional energy transfer,[7] scattering off a surface,[8] and photodissociation,[9] and has led to insight into the dynamics of these processes.

Consider a diatomic molecule in a $^1\Pi$ electronic state. In the absence of rotation there are two degenerate states represented by this term symbol, differing in their value of Λ ($\Lambda=\pm 1$). The electron probability density of the two states can be represented schematically by the orbitals labeled Π_X and Π_Y shown in Fig. 1(a) (where in addition a Σ orbital is shown). Now let the nuclei rotate about the X-axis. One of the Π-orbitals, Π_Y, lies in the plane of nuclear motion while the other does not. Nuclear rotation thus lifts the degeneracy of these two states; the resulting pair of eigenstates for the rotating molecule is called a Λ-doublet.

A common explanation for this energy splitting is that the electrons in the Π_Y state, unable to keep up with the rotating internuclear axis, lag behind, while the electrons in the Π_X state are not affected by the nuclear motion. This description of lagging orbitals was particularly spelled out in Ref. 6, and a picture similar to our Fig. 1(b) appears in Ref. 10. The picture seems plausible, since quantum theory asserts that the Π and Σ states are mixed, and since the superposition of a Π and a Σ state can produce a misaligned orbital.

In fact, this picture cannot be correct. One realizes this when seeking answers to the following questions: (1) What does the orthogonal combination of Π_Y and Σ states look like? and (2) What happens in the high-rotation limit? Concerning the latter question, the electronic states ought to go to degenerate space-fixed states with the nuclei twirling rapidly inside. How could misaligned states ever approach this limit?

The problem with the concept of a lagging orbital does not arise from the quantum formalism. For example, the equations for energy and wave functions given in Ref. 6 are perfectly correct. The problem arises because the quantum formulas are so opaque that it is hard to get an intuitive picture from them.

The goal of this paper is to provide a physical picture of Λ-doubling using the physical insight of semiclassical theory. These semiclassical results are then shown to be consistent with those of a more rigorous, full quantum model. In a subsequent paper we use this semiclassical model as a starting place to study collisional processes responsible for transitions between these Λ-doublet states.

In Sec. II we set up a semiclassical model of a diatomic molecule, obtain formulas for energies and wavefunctions, and obtain an intuitive physical picture of the Λ-doublet states. In Sec. III we show that the semiclassical theory gives (to good approximation) the same energy levels and wave functions as the full quantum theory, presented in brief form in the Appendix. Then, in Sec. IV, we use the semiclassical method to give the first examination of time-dependent states. We monitor expectation values of the electronic orbital-angular momentum vector, $\langle \mathbf{L} \rangle$, for an arbitrary state. Our present treatment does not include the influence of electron spin; this will be treated in a later paper.

Note that in addition to providing a physical picture of Λ-doubling in diatomic molecules, these semiclassical de-

 0021-9606/97/107(14)/5460/13/$10.00

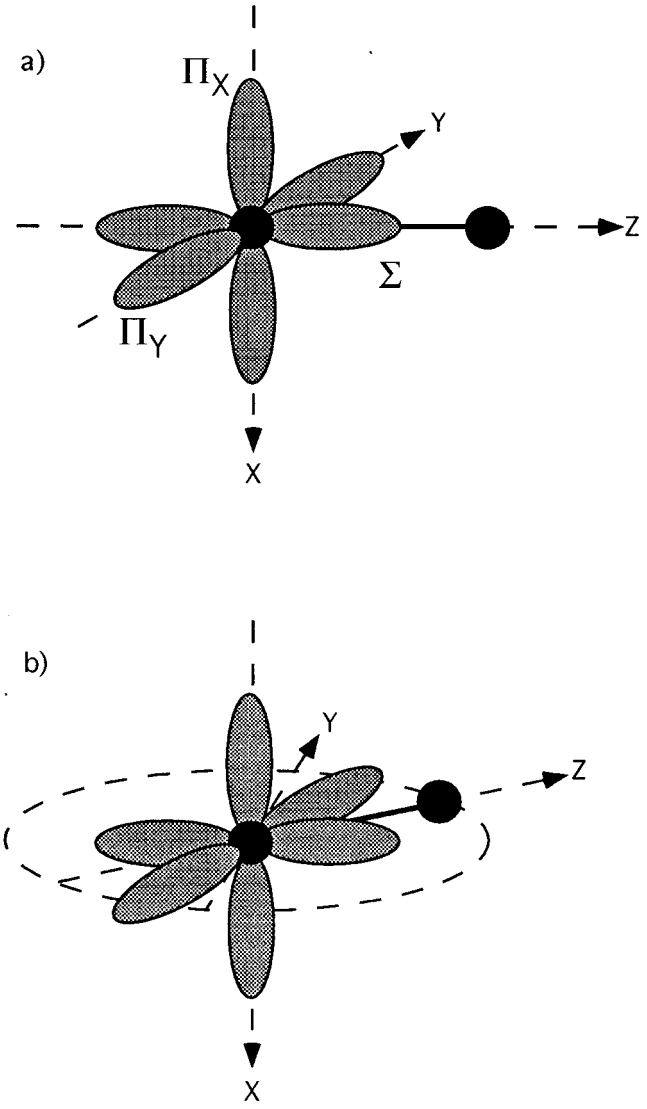

FIG. 1. (a) Schematic of three molecular orbitals (Π_X, Π_Y, Σ). The nuclei are represented by the two black dots on the Z axis. In the absence of nuclear rotation the two Π orbitals are indistinguishable and thus degenerate. (b) A common physical picture used to explain Λ-doubling in which the Π_Y and Σ orbitals are said to ''lag behind'' the rotating nuclear axis, thus losing some of their respective Π and Σ character, while the Π_X orbital does not need to adjust to the nuclear rotation to retain its Π symmetry.

scriptions, especially the time-dependent pictures, are needed to explore the mechanism of collision-induced transitions between these Λ-doublet states, presented in the accompanying paper.

II. SEMICLASSICAL MODEL

The model presented here is a modification of our previous work.[11] The diatomic molecule is treated as a three-particle system, consisting of two nuclei and an active electron. The motions of the nuclei are described by classical mechanics, while the motion of the active electron is described by quantum mechanics.

Let **R** be the internuclear vector, pointing from A to B and specified by its coordinates $\{R,\Theta,\Phi\}$, as shown in Fig. 2. Viewed from a frame in which the center of mass of the nuclei remains fixed, the relative motion of the nuclei can be described by the motion of a particle of reduced mass $\mu, = M_A M_B/(M_A+M_B)$.

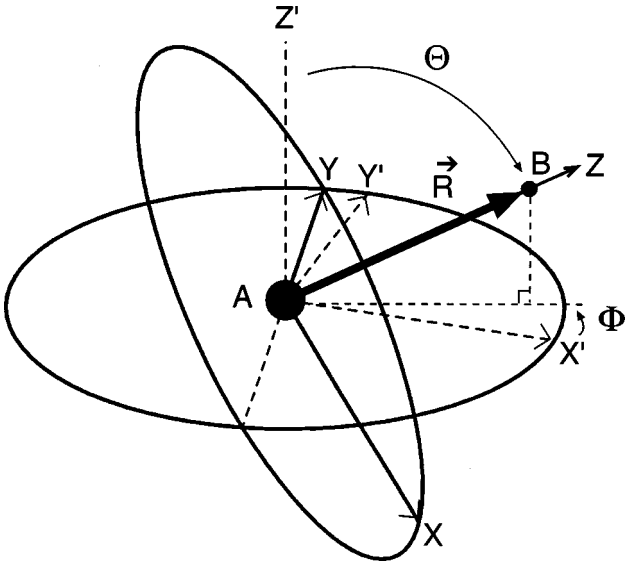

FIG. 2. The Euler angles Θ and Φ specifying the position of the internuclear vector, **R**, with respect to the space-fixed $\{X',Y',Z'\}$ frame. These angles also define the body-fixed $\{X,Y,Z\}$ frame, where the positive Z-axis is chosen along the internuclear axis, in the direction from A to B. Space-fixed coordinates are denoted by primes.

In this treatment we consider only the influence of nuclear rotation on electronic motion and so fix the internuclear distance, R, at its equilibrium value. For now we further simplify our model by restricting the nuclear rotation to a plane (we consider the effects of a three-dimensional nuclear trajectory in Sec. IV). Since the spatial orientation of the plane of nuclear rotation is arbitrary, we choose the plane of rotation to be the $X'Y'$ plane by setting $\Theta=90°$, leaving only one nonzero nuclear equation of motion[11]

$$\dot{\Phi} = \frac{N_{z'}}{\mu R^2}, \tag{1}$$

where $N_{Z'}$ is the projection of the nuclear angular momentum vector, **N**, on the Z' axis.[12]

Let $\mathbf{r}(r,\theta,\phi)$ be the vector representing the position of the active electron relative to the center of mass of the molecule; angles are defined relative to the internuclear axis, i.e., in the rotating frame. The electronic wave function $\Upsilon(\mathbf{r},t)$ satisfies a time-dependent Schrödinger equation,

$$i\hbar \frac{\partial \Upsilon(\mathbf{r},t)}{\partial t} = h_{\mathrm{el}} \Upsilon(\mathbf{r},t), \tag{2}$$

where h_{el} denotes the Born–Oppenheimer electrostatic electronic Hamiltonian.

We expand this wave function in the Born–Oppenheimer basis (eigenfunctions of h_{el}),

$$\Upsilon(\mathbf{r},t) = \sum_{\Lambda} c_{\Lambda}(t)|\Lambda\rangle = \sum_{\Lambda} c_{\Lambda}(t) F_{\Lambda}(r,\theta;\mathbf{R}) e^{i\Lambda\phi}, \tag{3}$$

and truncate this set to the three molecular states having the same electronic orbital-angular momentum $L=1$, the two Π states of interest and the closest Σ state. Phase conventions on angular momentum eigenstates are those of Condon and Shortley.[13]

The matrix representation of the Schrödinger equation for the electron in the Born–Oppenheimer basis is

$$i\hbar \frac{d}{dt}\underline{c}(t)=\{\underline{h}_{\rm el}+\dot{\Phi}\underline{L}_x\}\underline{c}(t), \tag{4}$$

where in addition to the electrostatic term, $\underline{h}_{\rm el}$, there is an angular coupling term, $\dot{\Phi}\underline{L}_x$, which arises because the basis functions are defined with respect to a rotating frame of reference.

The matrix elements of $\underline{h}_{\rm el}$ are diagonal and are the Born–Oppenheimer energies, ϵ_k, tabulated in Herzberg.[3] The angular coupling matrix elements are computed by expressing the operator L_x in terms of raising and lowering operators, L_+ and L_-. No general formula can be given for the matrix elements of $L_\pm$; however, selection rules for angular momentum components do hold[13] and can be expressed as

$$\langle\Lambda'|L_\pm|\Lambda\rangle=\delta_{\Lambda',\Lambda\pm1}\sqrt{2}\hbar Q, \tag{5}$$

where the parameter Q allows for the fact that the molecular basis functions differ from spherical harmonics. For our purposes, we set $Q=1$ in our numerical calculations.

A unitary transformation from the $\{|\Lambda\rangle,\Lambda=0,\pm1\}$ representation to the spatially-aligned $\{|\Pi_X\rangle,|\Pi_Y\rangle,|\Sigma\rangle\}$ representation converts the Hamiltonian matrix to block-diagonal form

$$\underline{h}_{\rm el}+\dot{\Phi}\underline{L}_x=\begin{pmatrix}\epsilon_\Pi & 0 & 0\\ 0 & \epsilon_\Pi & i\hbar\omega Q\\ 0 & -i\hbar\omega Q & \epsilon_\Sigma\end{pmatrix}, \tag{6}$$

where the rows and columns are labeled by the three basis functions $\{\Pi_X,\Pi_Y,\Sigma\}$. The Π_X orbital is uncoupled from the others. We note that this particular transformation produces purely real basis functions; this fact will be useful later in our interpretation of the Λ-doublet eigenfunctions.

The eigenvalues of this matrix are the ''electronic energy levels,''

$$e_\pm=\frac{\epsilon_\Sigma+\epsilon_\Pi}{2},$$
$$e_0=\epsilon_\Pi\sqrt{\left(\frac{\epsilon_\Sigma-\epsilon_\Pi}{2}\right)^2+(\hbar\omega Q)^2}. \tag{7}$$

The behavior of these electronic energy levels as a function of nuclear rotation rate is characterized by the ratio, δ, of the term characteristic of the angular coupling, $2\hbar\omega Q$, to the anisotropy of the electrostatic potential, $|\Delta\epsilon_{\Sigma,\Pi}|\equiv\epsilon_\Sigma-\epsilon_\Pi$,

$$\delta\equiv\frac{2\hbar\omega Q}{|\Delta\epsilon_{\Sigma,\Pi}|}. \tag{8}$$

Rewriting Eqs. (7) in terms of δ gives

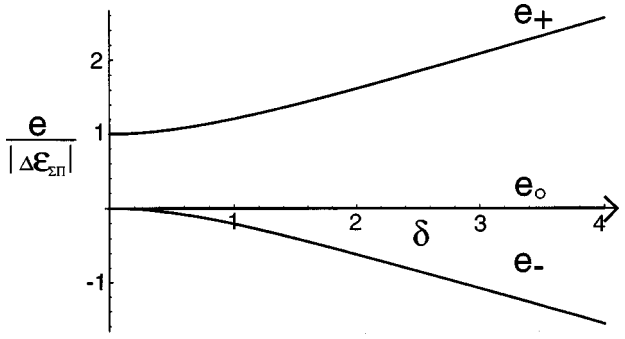

FIG. 3. Dependence of the semiclassical electronic energy levels on nuclear rotation rate for the three eigenstates. The energies are normalized with respect to the anisotropy of the potential, and are plotted vs δ, the ratio of the angular coupling to the anisotropy [see Eqs. (8) and (9)].

$$\frac{e_0}{|\Delta\epsilon_{\Sigma,\Pi}|}=0,\quad \frac{e_\pm}{|\Delta\epsilon_{\Sigma,\Pi}|}=\frac{1}{2}\pm\frac{\sqrt{1+\delta^2}}{2}, \tag{9}$$

where we define $\epsilon_\Pi=0$. The behavior of the electronic energy as a function of δ for each eigenstate is shown in Fig. 3. The energies of the Λ-doublets diverge with increasing rotation rate, while the energy of the uncoupled eigenstate remains constant. The energy splitting between the Λ-doublets becomes comparable to that between the Born–Oppenheimer Σ,Π states at around $\delta=3$.

We now look at the electronic eigenstates by plotting the angular dependence of $|\Upsilon|^2$, shown in Fig. 4. For the purposes of this section, we approximate the electronic basis functions as spherical harmonics. The angular dependence for the case of no nuclear rotation ($\delta=0$) is shown in Fig. 4(a), two Π orbitals and one Σ orbital. For $\delta=2$, shown in Fig. 4(b), the states are wider at their waists and have the shape of peanut shells. At higher δ, shown in Fig. 4(c) for $\delta=20$, they have become donut-shaped. In every case, the eigenfunctions have a symmetry with respect to the body-fixed axes. These eigenfunctions are not ''lagging.''

For further interpretation, we develop formulas for the electronic energies and wavefunctions in the limiting cases of high and low rate of rotation. Limiting behavior in the case of low rotation can be obtained by expanding the square root in Eq. (7) as a power series in δ. To first order in δ, for the case where $\epsilon_\Sigma>\epsilon_\Pi$,[14] the electronic energies are

$$e_0=\epsilon_\Pi,\quad e_-=\epsilon_\Pi-\delta\frac{\hbar\omega Q}{2},\quad e_+=\epsilon_\Sigma+\delta\frac{\hbar\omega Q}{2}, \tag{10}$$

and the associated eigenfunctions are

$$\Upsilon_0=|\Pi_X\rangle,$$
$$\Upsilon_-=\left(|\Pi_Y\rangle+\frac{i\delta}{2}|\Sigma\rangle\right)\frac{1}{\sqrt{1+\left(\frac{\delta}{2}\right)^2}}, \tag{11a}$$

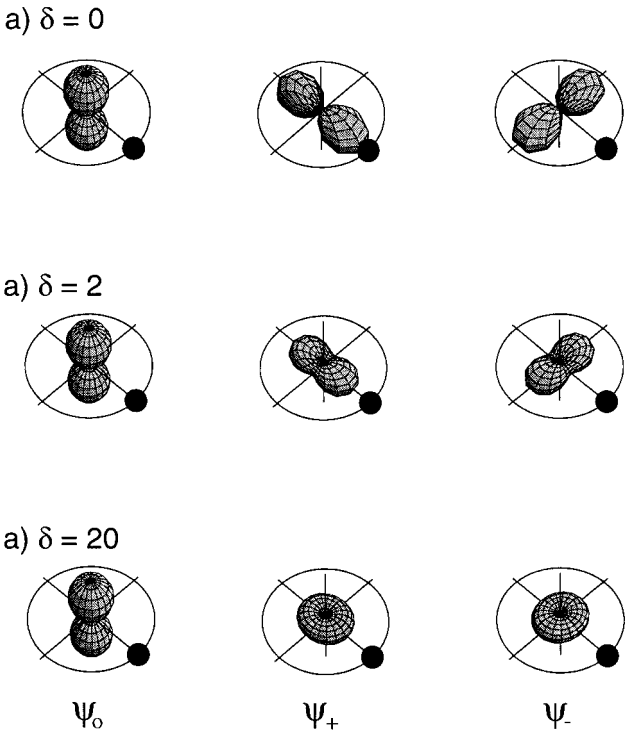

FIG. 4. Angular dependence of semiclassical electron probability densities for the three eigenstates at three nuclear rotation rates. (a) For the case of no rotation (δ=0), each eigenstate is a pure Born–Oppenheimer state, aligned along one of the molecular axes. (b) For moderate rotation (δ=2), the $\Psi_{\pm}$ eigenstates are mainly aligned states, with a travelling wave component. (c) For very high rotation (δ=20), the $\Psi_{\pm}$ eigenstates have become nearly pure traveling waves. In no case is there a ''misaligned'' eigenstate.

$$\Upsilon_+ = \left(|\Sigma\rangle + \frac{i\delta}{2}|\Pi_Y\rangle \right) \frac{1}{\sqrt{1+\left(\frac{\delta}{2}\right)^2}}.$$

We can rewrite the latter two of the above formulas in an equivalent form that allows for further interpretation:

$$\Upsilon_- = \left\{ \left(1-\frac{\delta}{2}\right)|\Pi_Y\rangle + i\,\frac{\delta}{2}\,[|\Sigma\rangle - i|\Pi_Y\rangle] \right\} \frac{1}{\sqrt{1+\left(\frac{\delta}{2}\right)^2}}, \tag{11b}$$

$$\Upsilon_+ = \left\{ \left(1-\frac{\delta}{2}\right)|\Sigma\rangle + i\,\frac{\delta}{2}\,[|\Pi_Y\rangle - i|\Sigma\rangle] \right\} \frac{1}{\sqrt{1+\left(\frac{\delta}{2}\right)^2}}.$$

Since the basis functions $|\Pi_X\rangle, |\Pi_Y\rangle$, and $|\Sigma\rangle$ are all real, the linear combinations $[|\Pi_Y\rangle - i|\Sigma\rangle]$ and $[|\Sigma\rangle - i|\Pi_Y\rangle]$ represent traveling waves. Thus Eqs. (11b) show that Υ_+ is a quantum superposition of mostly the aligned $|\Sigma\rangle$ state with a bit of a traveling wave state, $[|\Pi_Y\rangle - i|\Sigma\rangle]$.

We now consider the high rotation limit, this time by expanding the square root in Eq. (10) as a power series in $(1/\delta)$. To first order in $(1/\delta)$ the electronic energies are given by

$$e_0 = \epsilon_\Pi, \quad e_\pm = \frac{\epsilon_\Sigma + \epsilon_\Pi}{2} \pm \left(\hbar\omega Q + \frac{|\Delta\epsilon_{\Sigma\Pi}|}{4}\left[\frac{1}{\delta}\right] \right), \tag{12}$$

and the associated eigenfuntions by

$$\Upsilon_0 = |\Pi_X\rangle,$$

$$\Upsilon_- = \left\{ |\Pi_Y\rangle + i\left(1-\frac{1}{\delta}\right)|\Sigma\rangle \right\} \frac{1}{\sqrt{1+\left(1-\frac{1}{\delta}\right)^2}}, \tag{13}$$

$$\Upsilon_+ = \left\{ |\Sigma\rangle + i\left(1-\frac{1}{\delta}\right)|\Pi_Y\rangle \right\} \frac{1}{\sqrt{1+\left(1-\frac{1}{\delta}\right)^2}}.$$

The respective angular dependencies are shown in Fig. 4(b) for δ=2, where now the loss of the node along the Z axis is evident. Figure 4(c) shows angular dependencies for a much larger rotation rate, δ=20. In this high-δ limit the $\Upsilon_\pm$ eigenstates show no discernible angular dependence in the plane of rotation and are well represented by traveling waves. The nuclei are rotating so quickly that the electrons see an average potential energy, which is cylindrically symmetric about the X-axis. Accordingly, the eigenfunctions of the Hamiltonian are eigenfunctions of L_X with eigenvalues 0 or $\pm 1\hbar$.

To summarize, Λ-doublet wavefunctions do not lag behind the rotating internuclear axis; rather, they are superpositions of aligned Σ,Π states with travelling waves. In the low-rotation limit, the aligned component dominates, while in the high-rotation limit the travelling wave-component dominates.

We now use a more rigorous, full quantum model of the diatomic molecule to verify the results of the semiclassical model.

III. COMPARISON OF SEMICLASSICAL AND QUANTUM RESULTS

In order to compare the semiclassical energy levels with those from the full quantum model (see Appendix), we need to add to the semiclassical electronic eigenvalues the classical nuclear rotational energy,

$$e_{\rm rot} = \frac{\mu R^2 \omega^2}{2}. \tag{14}$$

To relate the resulting semiclassical total energies, which depend on ω, to the quantum energies, which are characterized by the quantum number K, we need to ''quantize'' ω. A reasonable choice is

$$\omega(K) = \frac{2B\sqrt{K(K+1)}}{\hbar}, \tag{15}$$

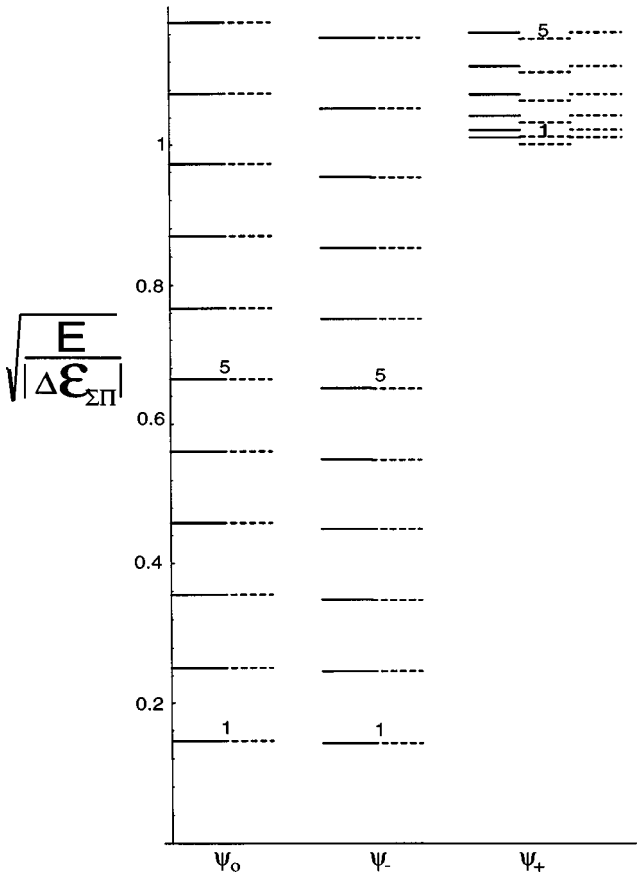

FIG. 5. Comparison of total energy levels for the three eigenstates calculated by the full quantum method (solid lines) and the semiclassical method using the approximate ''quantization'' of ω given in Eq. (15) (dotted lines). The energies are normalized with respect to the anisotropy of the potential. For ease of visualization we plot the square root of the energy. The value of K is written above selected energy levels. Agreement is especially good for the two Λ-doublet states, Ψ_0 and Ψ_-, though not so good for the Ψ_+ state. This discrepancy between the quantum and semiclassical energies for the Ψ_+ state can be reduced by adding a correction term of $2B$ to the semiclassical Ψ_+ (dot–dashed lines).

where the rotational energy constant $B = \hbar^2/(2\mu R^2)$. The resulting total energy levels for the semiclassical model, normalized to the anisotropy of the electrostatic potential, are then

$$\frac{E_0^{\mathrm{SC}}}{|\Delta\epsilon_{\Sigma,\Pi}|} = \frac{B}{|\Delta\epsilon_{\Sigma,\Pi}|}K(K+1),$$

$$\frac{E_\pm^{\mathrm{SC}}}{|\Delta\epsilon_{\Sigma,\Pi}|} = \frac{B}{|\Delta\epsilon_{\Sigma,\Pi}|}K(K+1)+\frac{1}{2} \pm \sqrt{\left(\frac{1}{2}\right)^2+4\left(\frac{BQ}{|\Delta\epsilon_{\Sigma,\Pi}|}\right)^2 K(K+1)}\,, \qquad (16)$$

and are shown along with the exact quantum energies in Fig. 5. As a consequence of this choice of $\omega(K)$, we find the following:

(i) The semiclassical quantity δ, defined in Eq. (8), is exactly equal to the quantum quantity Δ, defined in Eq. (A10).

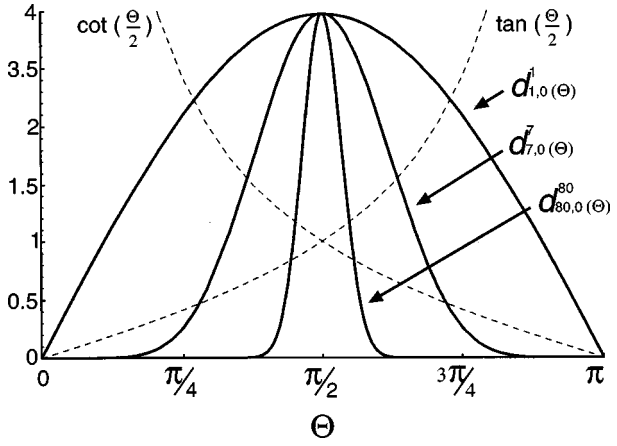

FIG. 6. Plot of Wigner-d functions for $K=1$, 7, and 80 (solid lines, in arbitrary units). These functions are highly peaked about $\Theta=\pi/2$ for high K, indicating localization of the nuclear wave functions near the X',Y' plane.

(ii) For the uncoupled state, the above semiclassical formula for the energy, E_0, is equivalent to the quantum formula, given in Eq. (A9).

(iii) The above semiclassical formulas for $E_\pm$ are quite close to the quantum formulas, given in Eq. (A9). This is illustrated in Fig. 5. On the scale of this figure we can see no difference between the quantum and semiclassical values for E_-. However, there is a small but visible discrepancy between the quantum and semiclassical values for E_+.

(iv) Much of this last discrepancy can be eliminated (if necessary) by adding the correction $2B$ to the eigenvalues E_+, as shown in Fig. 5.

We now compare semiclassical and quantum wavefunctions. The quantum expressions in Eqs. (A14) and (A17) contain Wigner-d functions as factors. A plot of three of these functions is shown in Fig. 6. One can show that the full width at half maximum (FWHM) of the d-function, for large K, is given by

$$\mathrm{FWHM}=2\left[90^\circ-\arcsin\left(\frac{1}{K/\sqrt{2}}\right)\right]. \qquad (17)$$

For high K, the d-function is seen to be highly peaked about $\Theta=90°$, representing localization of the nuclei near the $X'Y'$ plane, consistent with the semiclassical model. Since this factor causes the eigenfunctions to be nonzero only near $\Theta=90°$, we can simplify the expressions for the wave functions by replacing the $\cot(\Theta/2)$ and $\tan(\Theta/2)$ factors in Eqs. (A14) and (A17) by their values at $\Theta=90°$. In addition, we make a further approximation by replacing $[K/(K+1)]^{1/2}$ with unity. The high-K quantum eigenfunctions of Eq. (A17) then become

$$\Psi_0^{E,K,M} = -e^{iK\Phi} d^K_{K,0}(\Theta)|\Pi_x\rangle,$$

$$\Psi_-^{E,K,M} = \frac{-e^{iK\Phi} d^K_{K,0}(\Theta)}{\sqrt{1+\left(1-\frac{1}{\Delta}\right)^2}}\left[|\Pi_y\rangle + i\left(1-\frac{1}{\Delta}\right)|\Sigma\rangle\right], \tag{18}$$

$$\Psi_+^{E,K,M} = \frac{e^{iK\Phi} d^K_{K,0}(\Theta)}{\sqrt{1+\left(1-\frac{1}{\Delta}\right)^2}}\left[|\Sigma\rangle + i\left(1-\frac{1}{\Delta}\right)|\Pi_y\rangle\right],$$

where these eigenfunctions are now separated into nuclear and electronic factors. These quantum electronic factors are identical to the semiclassical electronic eigenfunctions in Eq. (13).

In Fig. 4, we used the semiclassical wave functions to plot electronic angular probability distributions. Alternatively, we can use the full quantum wave functions to obtain conditional probability distributions for finding the electron in a particular solid angle given that the nuclei are found in the $X'Y'$ plane ($\Theta = 90°$). These quantum angular distributions are identical to the semiclassical angular distributions.

Similar approximations can be made for the quantum eigenfunctions in the low-K limit, though we are constrained in how low we can go. As seen in Fig. 6, it is still reasonable to approximate $\cot(\Theta/2) \cong \tan(\Theta/2) \cong 1$ for $K=7$. However, this would not be a reasonable approximation for $K=1$; the nuclei are not localized near the $X'Y'$ plane for such a low value of K. This approximation gives

$$\Psi_0^{E,K,M} = -e^{iK\Phi} d^K_{K,0}(\Theta)|\Pi_X\rangle,$$

$$\Psi_-^{E,K,M} = \frac{e^{iK\Phi} d^K_{K,0}(\Theta)}{\sqrt{1+\left(\frac{\Delta}{2}\right)^2}}\left[|\Pi_Y\rangle + i\,\frac{\Delta}{2}\,|\Sigma\rangle\right], \tag{19}$$

$$\Psi_+^{E,K,M} = \frac{e^{iK\Phi} d^K_{K,0}(\Theta)}{\sqrt{1+\left(\frac{\Delta}{2}\right)^2}}\left[|\Sigma\rangle + i\,\frac{\Delta}{2}\,|\Pi_Y\rangle\right],$$

where these formulas should be satisfactory for $4 \leqslant K \ll |\Delta\epsilon_{\Sigma,\Pi}|/(4BQ)$. Here the upper limit comes from setting $\Delta \ll 1$ in Eq. (A10). For the low-K limit too, these quantum electronic factors are identical to the semiclassical electronic wave functions in Eq. (11).

IV. DYNAMICS OF TIME-DEPENDENT STATES

Let us now examine time-dependent states of the molecule. These pictures will be especially helpful for our study of collision processes in the accompanying paper. We monitor the expectation value of the electronic orbital-angular momentum vector, $\langle \mathbf{L} \rangle$, as a function of time. We choose the initial electronic state so that we can easily see the time-evolution of $\langle \mathbf{L} \rangle$; in particular we choose the Born–Oppenheimer basis function $|\Lambda\rangle = |-1\rangle$, so that $\langle \mathbf{L} \rangle$ starts out along the negative Z axis. We begin by using planar nuclear trajectories, with ω given by Eq. (4).

We first consider the case of low rotation rate, corresponding to $K=7$. Integration of Eq. (4) gives the result shown from a space-fixed point of view in Fig. 7(a), and from a molecule-fixed point of view in Fig. 7(b) The molecule has undergone 3/4 of a rotation in 1 ps, during which time $\langle \mathbf{L} \rangle$ has undergone approximately 5 precessions about the internuclear axis. Thus the projection of $\langle \mathbf{L} \rangle$ onto the internuclear axis, $\langle L_Z \rangle$, is fixed. We say $\langle \mathbf{L} \rangle$ is ''locked'' onto the internuclear axis. The frequency of precession depends on the anisotropy of the electrostatic potential, and is given by $|\Delta\epsilon_{\Sigma,\Pi}|/\hbar$. The same trajectory is shown in Fig. 7(c) over a longer time duration of 7 ps, from which it is seen that $\langle L_Z \rangle$ is actually slowly oscillating. The frequency for this oscillation depends on the energy splitting between the Λ-doublets, and is equal to $\{|e_0 - e_-|/\hbar\} \cong \{\hbar\omega^2/|\Delta\epsilon_{\Sigma,\Pi}|\}$ by Eqs. (8) and (9). This figure also shows that $\langle \mathbf{L} \rangle$ is precessing nearly, but not quite, about the internuclear axis; $\langle \mathbf{L} \rangle$ seems to ''hover'' just above the axis. A top view of the same trajectory, as viewed from along the negative X-axis, is shown in Fig. 7(d). Here $\langle \mathbf{L} \rangle$ is seen to ''wag'' from one side of the X axis to the other. The origin of this wag is the precession of $\langle \mathbf{N} \rangle$ and $\langle \mathbf{L} \rangle$ about the total angular momentum $\langle \mathbf{K} \rangle$, as shown later in this section. The rate of wag is 2ω, twice the rotation rate.

Now consider a rapidly rotating molecule, by setting $K = 500$. Figure 8(a) shows the molecule undergoing about 3/4 of a rotation in a much shorter time, 0.015 ps, while $\langle \mathbf{L} \rangle$ remains nearly space-fixed. Since the precession rate, characteristic of the anisotropy of the electrostatic potential, is the same as before, $\langle \mathbf{L} \rangle$ has undergone only a small fraction of a precession in this time, barely discernible from the picture. Thus in this case the molecule is rotating far too quickly for $\langle \mathbf{L} \rangle$ to follow, and we say $\langle \mathbf{L} \rangle$ is ''decoupled'' from the internuclear axis. The view from the rotating molecular frame, Fig. 8(b), gives another perspective. Since $\langle \mathbf{L} \rangle$ rotates approximately 3/4 of a revolution in 0.015 ps, the projection of $\langle \mathbf{L} \rangle$ onto the molecular Z axis oscillates. This oscillation frequency is still related to the ''Λ-doublet splitting,'' and is equal to $(e_0 - e_-)/\hbar$. In this high-K limit this Λ-doublet splitting approaches the nuclear rotation frequency. Returning to a view from the space-fixed frame, and following the trajectory for a longer time, 0.75 ps, we see in Fig. 8(c) that $\langle \mathbf{L} \rangle$ slowly oscillates along the space-fixed X' axis, with a frequency of oscillation given by $|\Delta\epsilon_{\Sigma,\Pi}|/(2\hbar)$. The difference $|\Delta\epsilon_{\Sigma,\Pi}|/2$ is the energy gap, $E_-(K+1) - E_0(K) \approx E_+(K-1) - E_0(K)$, between Υ_0 and the nearest $\Upsilon_\pm$ states. This energy gap arises from the anisotropy of the potential energy felt by the electron in the space-fixed frame, produced by the nuclei that are rapidly rotating in the $X'Y'$ plane. Note also that the line on which $\langle \mathbf{L} \rangle$ oscillates slowly rotates. The motion of $\langle \mathbf{L} \rangle$ in the space-fixed frame then has the appearance of the motion of a Foucault pendulum.

If we consider an intermediate case, a value of K where the precession rate is comparable to the oscillation rate, ($K = 80$), we get the trajectory shown in Fig. 9, shown from a

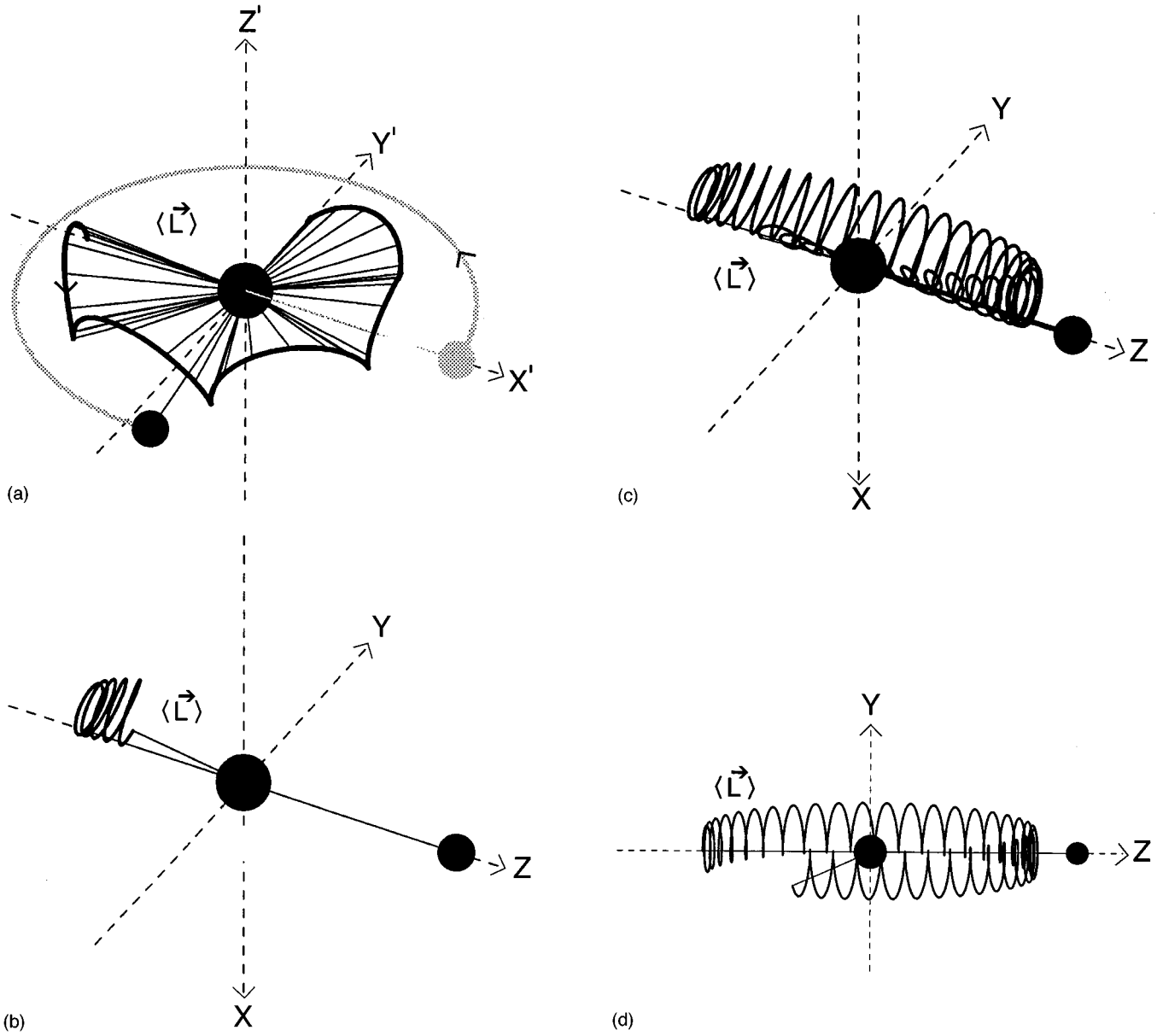

FIG. 7. Behavior of the expectation value of electronic orbital-angular momentum $\langle \mathbf{L} \rangle$ for low rotation ($K=7$). A planar nuclear trajectory is used. (a) A typical trajectory is shown in the space-fixed frame with atom A at the origin. The initial position of the molecular axis is shown in gray, the final position in black, from which it is seen that the molecule undergoes about 3/4 of a rotation in 1 ps. Several snapshots of the vector $\langle \mathbf{L} \rangle$ are shown. The heavy black line shows the locus of the tips of this vector, which starts out along the negative X' axis and ends up along the positive Y' axis. This behavior can be better understood by looking at (b) in which the same trajectory is shown but in the body-fixed frame. It is evident that $\langle \mathbf{L} \rangle$, which starts out along the internuclear axis, (negative Z-axis), precesses approximately five times about that axis. The same trajectory is shown in (c) for the body-fixed frame over a longer time duration, 7 ps, during which time $\langle L_Z \rangle$ is seen to have undergone almost one complete oscillation along the internuclear axis. Also note that $\langle \mathbf{L} \rangle$ has a component of angular momentum along the negative X-axis, the axis of rotation. A top view of the same trajectory, as viewed from along the negative X-axis, is shown in (d). Here $\langle \mathbf{L} \rangle$ is seen to ''wag'' from one side of the X axis to the other.

space-fixed point of view. The behavior of $\langle \mathbf{L} \rangle$ is complicated. Over the 9 ps duration of this trajectory, $\langle \mathbf{L} \rangle$ has undergone about 4 precessions while $\langle L_Z \rangle$ has undergone about 5 oscillations. To aid in visualizing the motion of $\langle \mathbf{L} \rangle$, progressive positions of $\langle \mathbf{L} \rangle$ are numbered in the figure.

By considering planar nuclear trajectories, we have avoided the question of how the electronic motion affects the nuclear motion, which we now address. Using the method described in our previous paper,[11] we generate a 3D nuclear trajectory such that both total energy and total angular momentum are conserved. In addition to monitoring $\langle \mathbf{L} \rangle$ as a function of time, we also monitor the expectation values of both the total angular momentum, $\langle \mathbf{K} \rangle$, and the nuclear angular momentum $\langle \mathbf{N} \rangle$. The result is shown in Fig. 10(a) in the low rotation limit ($K=7$) for the same set of initial conditions used to generate the planar trajectory results of Fig. 7. It is seen that $\langle \mathbf{N} \rangle$ and $\langle \mathbf{L} \rangle$ precess about a space-fixed $\langle \mathbf{K} \rangle$ with a period equal to the rate of rotation. Thus $\langle \mathbf{L} \rangle$ is not

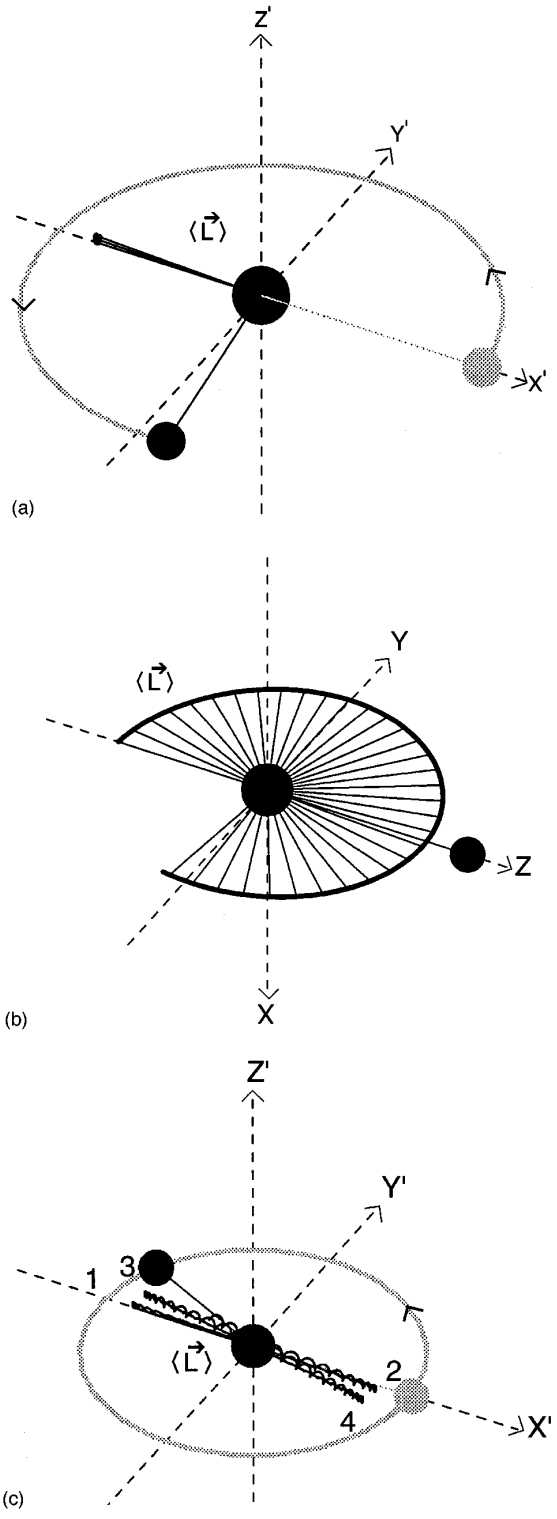

FIG. 8. Behavior of the expectation value of electronic orbital-angular momentum $\langle \mathbf{L} \rangle$ for high rotation ($K=500$). A planar nuclear trajectory is used. (a) A typical trajectory is shown in the space-fixed frame. The molecule has undergone about 3/4 of a rotation in 0.015 ps, during which time $\langle \mathbf{L} \rangle$ remains nearly space-fixed. In (b) the same trajectory is shown but in the body-fixed frame. Note that the projection of $\langle \mathbf{L} \rangle$ on the rotating Z axis, $\langle L_Z \rangle$, is oscillating at the same frequency as the nuclear rotation frequency. The same trajectory is shown in (c) for the space-fixed frame over a longer time duration, 0.75 ps. Here $\langle \mathbf{L} \rangle$ is seen to oscillate along a nearly space-fixed axis on a time scale of about 0.2 ps, while that axis itself slowly rotates. The motion of $\langle \mathbf{L} \rangle$ is thus like a Foucault pendulum, with successive positions of $\langle \mathbf{L} \rangle$ indicated in the figure with the numbers 1–4.

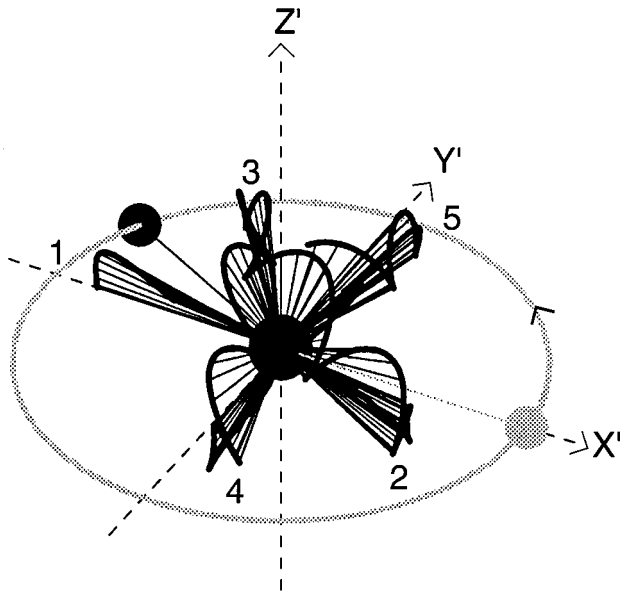

FIG. 9. Behavior of the expectation value of electronic orbital-angular momentum, $\langle \mathbf{L} \rangle$, for intermediate rotation ($K=80$), where the precession frequency of $\langle \mathbf{L} \rangle$ about the internuclear axis is comparable to the oscillation frequency of its projection along the same axis. A planar nuclear trajectory is used. The molecule undergoes about 7 or 8 rotations in 0.9 ps. The motion of $\langle \mathbf{L} \rangle$ appears analogous to that of a Focault pendulum. It starts in region 1, oscillates nearly along the X' axis to region 2, then over to 3, and so on.

only precessing rapidly about the internuclear axis but also more slowly about the total angular momentum. Figure 10(b) shows the same trajectory, viewed in the body-fixed frame. The qualitative behavior of $\langle \mathbf{L} \rangle$ is similar to that shown for the planar trajectory in Fig. 7(c). The nuclear angular momentum, $\langle \mathbf{N} \rangle$, which must by definition be perpendicular to the z axis, is always found nearly along the X axis, the initial axis of nuclear rotation. In fact, $\langle \mathbf{N} \rangle$ oscillates with small amplitude in the xy plane about the X axis, causing the total angular momentum, $\langle \mathbf{K} \rangle$, to oscillate accordingly.

There is one qualitative difference in the electronic motion for planar trajectories as compared with 3D trajectories and it is present only in the low K limit. In the former case, $\langle L_Z \rangle$ always oscillates at a frequency given by the Λ-doublet splitting, while in the latter case conservation laws may prevent $\langle L_Z \rangle$ from oscillating. This constraint can be seen in Fig. 11 ($K=1$), where $\langle \mathbf{L} \rangle$ is seen always to point away from atom A, such that $\langle L_Z \rangle$ is always along the negative Z axis. Imagine now that $\langle L_Z \rangle$ were to lie along the positive Z axis, which would be the case if it underwent half of an oscillation. The electronic energy for this hypothetical state would be nearly the same, and thus, by energy conservation, the length of $\langle \mathbf{N} \rangle$ would have to be nearly the same. Yet since $\langle \mathbf{L} \rangle$ would point in a different direction from the original $\langle \mathbf{L} \rangle$, the resultant of $\langle \mathbf{L} \rangle$ and $\langle \mathbf{N} \rangle$ would be very different from the initial $\langle \mathbf{K} \rangle$. But by conservation of total angular momentum, $\langle \mathbf{K} \rangle$ must be constant. Thus oscillation of $\langle \mathbf{L} \rangle$ along the internuclear axis for such a small value of K would violate conservation of total angular momentum and so $\langle L_Z \rangle$ is constrained in its range of oscillation.

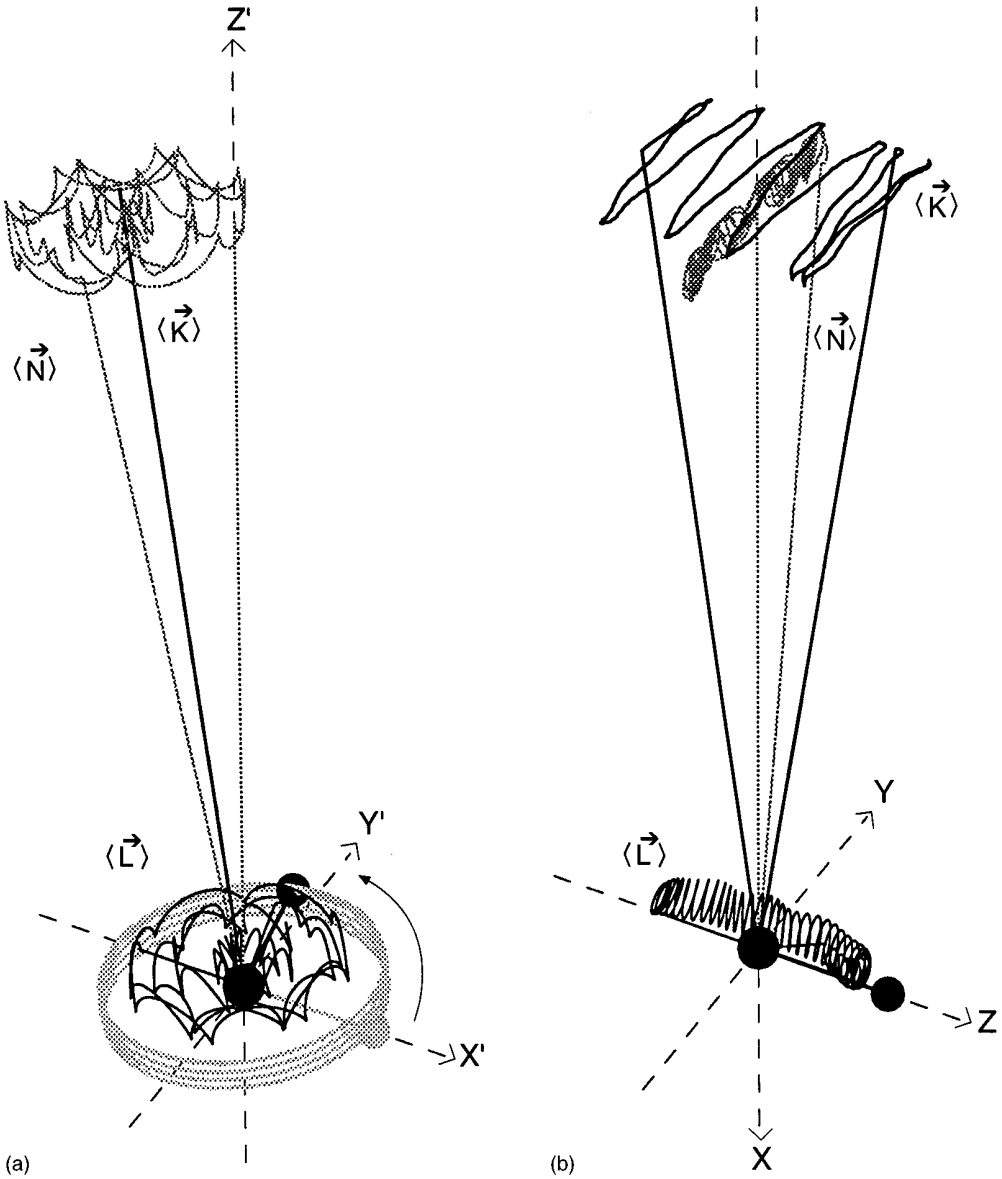

FIG. 10. Behavior of $\langle \mathbf{L} \rangle$ and the expectation value of nuclear angular momentum, $\langle \mathbf{N} \rangle$, accounting for conservation of total energy and angular momentum. A typical trajectory for low rotation ($K=7$) is shown in (a) the space-fixed frame and (b) the body-fixed frame. The time duration is 7 ps, which corresponds to approximately $4\frac{1}{4}$ nuclear rotations. In the body-fixed frame, $\langle \mathbf{L} \rangle$ is seen to undergo a spiraling motion, corresponding to fast precession about the rotating axis and slower oscillation along that axis. This behavior is qualitatively similar to that obtained for the planar nuclear trajectory shown in Fig. 7(c). Also in the body-fixed frame, the nuclear angular momentum vector, $\langle \mathbf{N} \rangle$, though always perpendicular to the Z-axis, is not constant; rather, it oscillates in the XY plane about the negative X-axis. In the space-fixed frame, the nuclear angular momentum vector, $\langle \mathbf{N} \rangle$, is seen to adjust to the motion of $\langle \mathbf{L} \rangle$ such that the total angular momentum, $\langle \mathbf{K} \rangle$, remains fixed. The nuclear trajectory is seen to be nearly planar.

This is not a problem for large enough K. As K increases, so does the length of $\langle \mathbf{N} \rangle$, while the length of $\langle \mathbf{L} \rangle$ is constrained to be less than or equal to 1. Thus $\langle \mathbf{K} \rangle$ becomes nearly coincident with $\langle \mathbf{N} \rangle$, which is perpendicular to the diatomic axis. Then oscillation of $\langle L_Z \rangle$ causes a much smaller relative change in the length of $\langle \mathbf{N} \rangle$, enabling both energy and angular momentum to be conserved. Consider the case $K=7$, as shown in Fig. 10(b). $\langle L_Z \rangle$ oscillates its full range, and the electronic motion as viewed from the molecular frame is nearly the same as for the planar case.

V. CONCLUSION

We have obtained a semiclassical picture of Λ-doubling, one which is consistent with a full quantum treatment, but which gives a more intuitive, pictorial view of the dynamics. We see that ''lagging'' of oriented orbitals behind the rotating internuclear axis is not a correct description of the states; rather, the decoupling of the electronic motion from the nuclear axis is represented by states which can be interpreted as a superposition of aligned states and traveling waves.

We have investigated how the expectation value of electronic orbital-angular momentum, $\langle \mathbf{L} \rangle$, changes with time for different nuclear rotation rates. We see that not only does $\langle \mathbf{L} \rangle$ precess about the nuclear axis, but its projection along that axis oscillates.

We have shown that in most cases, the behavior of $\langle \mathbf{L} \rangle$ for a planar nuclear trajectory is similar to that for a 3D

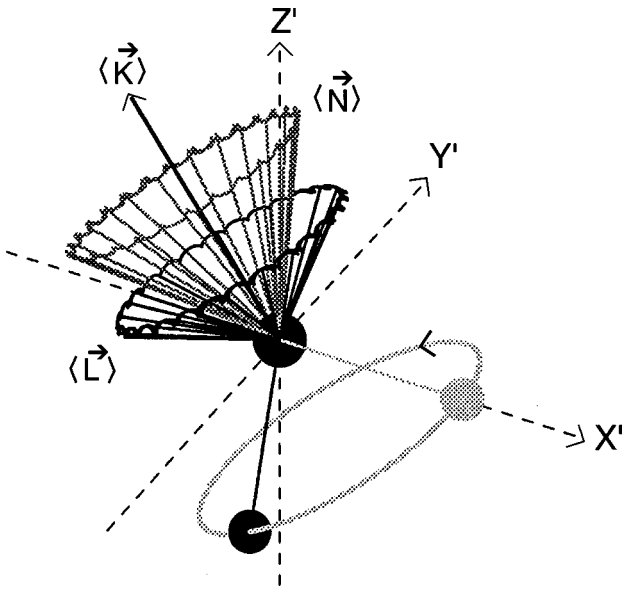

FIG. 11. A three-dimensional trajectory conserving total energy and angular momentum for $K=1$. In this case the nuclei do not rotate in a plane. Instead, the twirling internuclear axis traces out a cone. Also, $\langle L_Z\rangle$ cannot oscillate significantly along the internuclear axis. It is restricted by conservation of total angular momentum and energy.

trajectory in which energy and total angular momentum are conserved; however, we have identified one regime, very low K, in which the behavior differs qualitatively from that for a 3D trajectory. Specifically, we saw that for large K, $\langle L_Z\rangle$ oscillates between approximately $+\Lambda$ and $-\Lambda$, while for small K the range of oscillation of $\langle L_Z\rangle$ is smaller.

Now that we have verified the results of the semiclassical model, we use this semiclassical theory in the accompanying paper to obtain insight into the dynamics of collisionally-induced electronic transitions in oriented diatomic molecules.

ACKNOWLEDGMENTS

This research was funded by both the American Chemical Society-Petroleum Research Fund and a William and Flora Hewlett Foundation Award of Research Corporation through grants to Eckerd College, and by NSF and ONR through grants to the College of William and Mary. We also want to gratefully acknowledge support by JILA where part of this work was completed. L.J.K. also thanks Steve Leone for valuable comments on the manuscript, and Neil York for help with computer programming.

APPENDIX: FULL QUANTUM MODEL

Here we review the quantum theory of Λ-doubling, setting it up in a way that will make it easy to compare with the corresponding semiclassical description given in Sec. II.

The Hamiltonian for the total system is given by

$$H=-\frac{\hbar^2}{2\mu}\nabla_R^2+h_e. \tag{A1}$$

The wave function $\Psi^{E,K,M}$ for the full system of electrons and nuclei is an eigenfunction of H and of both the square of the total angular momentum operator, K^2, with eigenvalue $K(K+1)\hbar^2$, and the projection of the total angular momentum onto a space-fixed axis, $K_{Z'}$, with eigenvalue $M\hbar$.

We expand the eigenfunction $\Psi^{E,K,M}$ in terms of basis functions which are products of Born–Oppenheimer electronic eigenfunctions, $\phi_\Lambda(\mathbf{r};\mathbf{R})$, nuclear vibrational factors, $u(R)/R$, and symmetric-top eigenfunctions, $D^{K*}_{M\Lambda}(\Phi,\Theta,0)$,

$$\Psi^{EKM}=\sum_\Lambda c_\Lambda\left(\frac{u(R)}{R}\right)D^{K*}_{M\Lambda}(\Phi,\Theta,0)\,\phi_\Lambda(\mathbf{r};\mathbf{R}). \tag{A2}$$

We use an ''active'' notation for the nuclear angular factor[15]

$$\begin{aligned} &D^{K*}_{M\Lambda}(\Phi,\Theta,0)=e^{iM\Phi}d^{K*}_{M\Lambda}(\Theta),\\ &d^{K*}_{M\Lambda}(\Theta)=\langle K,M|e^{-iK_Y\Theta\hbar}|K,\Lambda\rangle. \end{aligned} \tag{A3}$$

Since the molecule is cylindrically symmetric, the choice of the third Euler angle, χ, in the $D(\Phi,\Theta,\chi)$, is arbitrary.[16] We choose $\chi=0$.

Substituting the expansion of $\Psi^{E,K,M}$ into the full Schrödinger equation and following the procedure in Delos,[17] gives

$$\sum_\Lambda c_\Lambda\left\{\begin{array}{l} \delta_{\Lambda',\Lambda}\left[\begin{array}{l} \dfrac{\hbar^2}{2\mu}\dfrac{\partial^2}{\partial R^2}+\langle\phi_{\Lambda'}|h_{\rm el}|\phi_\Lambda\rangle-E\\ +\dfrac{\hbar^2}{2\mu R^2}[K(K+1)-\Lambda^2]\\ +\dfrac{1}{2\mu R^2}(\langle\phi_{\Lambda'}|L^2|\phi_\Lambda\rangle-\Lambda^2\hbar^2)\end{array}\right]\\ -\delta_{\Lambda',\Lambda+1}\left\{\dfrac{\hbar^2}{2\mu R^2}\sqrt{[(K+\Lambda+1)(K-\Lambda)]}\langle\phi_{\Lambda'}|L_+|\phi_\Lambda\rangle\right\}\\ -\delta_{\Lambda',\Lambda-1}\left\{\dfrac{\hbar^2}{2\mu R^2}\sqrt{[(K-\Lambda+1)(K+\Lambda)]}\langle\phi_{\Lambda'}|L_-|\phi_\Lambda\rangle\right\}\end{array}\right\}u=0. \tag{A4}$$

To express this in block-diagonalized matrix form we transform the basis set to the linear combinations

$$\gamma_1=\frac{1}{\sqrt{2}}\left[-D^{K*}_{M,1}|1\rangle+D^{K*}_{M,-1}|-1\rangle\right],\quad \gamma_2=\frac{-1}{i\sqrt{2}}\left[D^{K*}_{M,1}|1\rangle+D^{K*}_{M,-1}|-1\rangle\right],\quad \gamma_3=D^{K*}_{M,0}|0\rangle, \tag{A5}$$

using the same transformation as in the semiclassical treatment. The resulting matrix representation of the secular equation is then given by

$$\begin{vmatrix} (E_R+E_K+\epsilon'_\Pi-E) & 0 & 0 \\ 0 & (E_R+E_K+\epsilon'_\Pi-E) & -i2BQ\sqrt{K(K+1)} \\ 0 & i2BQ\sqrt{K(K+1)} & (E_R+E_K+\epsilon'_\Sigma)-E \end{vmatrix}=0, \tag{A6}$$

where we have used the following definitions:[18]

$$\begin{aligned} E_R&\equiv\frac{-\hbar^2}{2\mu u}\frac{\partial^2 u}{\partial R^2},\quad E_K\equiv BK(K+1),\\ \epsilon'_\Pi&\equiv\epsilon_\Pi-2B+\frac{\langle 1,1|L^2|1,1\rangle}{2\mu R^2},\\ \epsilon'_\Sigma&\equiv\epsilon_\Sigma+\frac{\langle 1,0|L^2|1,0\rangle}{2\mu R^2},\quad B=\frac{\hbar^2}{2\mu R^2}. \end{aligned} \tag{A7}$$

Energy levels, found by solving this secular equation, are

$$\begin{aligned} E_0&=E_R+E_K+\epsilon'_\Pi,\\ E_\pm&=E_R+E_K+\left(\frac{\epsilon'_\Pi+\epsilon'_\Sigma}{2}\right)\\ &\quad\pm\sqrt{\left(\frac{\epsilon'_\Sigma-\epsilon'_\Pi}{2}\right)^2+(2BQ)^2K(K+1)}\ . \end{aligned} \tag{A8}$$

The first term, E_R, corresponds to radial, or vibrational, energy. This is an additive constant to all energy levels, so we ignore it. In these expressions there is one relevant parameter which depends on the particular molecule, the ratio of the anisotropy of the electrostatic potential, $\epsilon_\Sigma-\epsilon_\Pi\equiv|\Delta\epsilon|$, to the rotational energy constant, B. Therefore, to see how these eigenvalues vary with nuclear rotation, we divide these equations by $|\Delta\epsilon|$,

$$\begin{aligned} \frac{E_0}{|\Delta\epsilon|}&=\frac{B}{|\Delta\epsilon|}K(K+1),\\ \frac{E_\pm}{|\Delta\epsilon|}&=\frac{B}{|\Delta\epsilon|}K(K+1)+\left(\frac{1}{2}+\frac{B}{|\Delta\epsilon|}\right)\\ &\quad\pm\sqrt{\left(\frac{1}{2}+\frac{B}{|\Delta\epsilon|}\right)^2+4\left(\frac{BQ}{|\Delta\epsilon|}\right)^2K(K+1)}\ . \end{aligned} \tag{A9}$$

Here we have defined the zero of energy to be ϵ_Π, consistent with the semiclassical treatment. These energy levels are the solid lines shown in Fig. 5.

We now derive formulas for energy levels and eigenfunctions in the two limits of low and high K. The limiting behavior for low values of K is obtained by expanding the square root in Eq. (A8) as a power series in Δ,

$$\Delta=\frac{4BQ\sqrt{K(K+1)}}{|\Delta\epsilon|}. \tag{A10}$$

To first order in Δ, the energy levels are given by the familiar formulas

$$\begin{aligned} E_0&=BK(K+1),\\ E_-&=BK(K+1)+\epsilon'_\Pi-BQ\sqrt{K(K+1)}\Delta,\\ E_+&=BK(K+1)+\epsilon'_\Sigma+BQ\sqrt{K(K+1)}\Delta, \end{aligned} \tag{A11}$$

and the associated wave functions by

$$\Psi_0^{E,K,M}=\left(\frac{-D^{K*}_{K,1}|1\rangle+D^{K*}_{K,-1}|-1\rangle}{\sqrt{2}}\right),$$

$$\begin{aligned} \Psi_-^{E,K,M}\cong\frac{1}{\sqrt{1+\left(\frac{\Delta}{2}\right)^2}}\Bigg[&-\left(\frac{-D^{K*}_{K,1}|1\rangle-D^{K*}_{K,-1}|-1\rangle}{i\sqrt{2}}\right)\\ &+\frac{i\Delta}{2}\left(D^{K*}_{K,0}|0\rangle\right)\Bigg], \end{aligned} \tag{A12}$$

$$\begin{aligned} \Psi_+^{E,K,M}\cong\frac{1}{\sqrt{1+\left(\frac{\Delta}{2}\right)^2}}\Bigg[&\frac{-i\Delta}{2}\left(\frac{-D^{K*}_{K,1}|1\rangle-D^{K*}_{K,-1}|-1\rangle}{i\sqrt{2}}\right)\\ &+\left(D^{K*}_{K,0}|0\rangle\right)\Bigg]. \end{aligned}$$

Anticipating comparison with semiclassical results, we rewrite this in an equivalent form for the particular case of $M=K$, in which the projection of total angular momentum along the space-fixed Z' axis is as large as possible. (The choice of M is arbitrary.) Substituting Eq. (A3) into Eq. (A12) and using the following expression[19] for Wigner-d's with $M=K$:

$$d^K_{K,\Lambda}(\Theta)=(-1)^{K-\Lambda}\sqrt{\frac{(2K)!}{(K+\Lambda)!(K-\Lambda)!}}\times\left[\cos\left(\frac{\Theta}{2}\right)\right]^{K+\Lambda}\left[\sin\left(\frac{\Theta}{2}\right)\right]^{K-\Lambda}, \tag{A13}$$

we obtain the following equivalent expressions for the low-K limit wave functions of Eq. (A12):

$$\Psi_0^{E,K,M}=e^{iK\Phi}d^K_{K,0}(\Theta)\sqrt{\frac{K}{K+1}}\times\left[\frac{\cot\left(\frac{\Theta}{2}\right)|1\rangle-\tan\left(\frac{\Theta}{2}\right)|-1\rangle}{\sqrt{2}}\right],$$

$$\Psi_-^{E,K,M}=\frac{e^{iK\Phi}d^K_{K,0}(\Theta)}{\sqrt{1+\left(\frac{\Delta}{2}\right)^2}}\left\{\sqrt{\frac{K}{K+1}}\times\left[\frac{-\cot\left(\frac{\Theta}{2}\right)|1\rangle-\tan\left(\frac{\Theta}{2}\right)|-1\rangle}{i\sqrt{2}}\right]+\frac{i\Delta}{2}|0\rangle\right\}, \tag{A14}$$

$$\Psi_+^{E,K,M}=\frac{e^{iK\Phi}d^K_{K,0}(\Theta)}{\sqrt{1+\left(\frac{\Delta}{2}\right)^2}}\left\{\frac{i\Delta}{2}\sqrt{\frac{K}{K+1}}\times\left[\frac{-\cot\left(\frac{\Theta}{2}\right)|1\rangle-\tan\left(\frac{\Theta}{2}\right)|-1\rangle}{i\sqrt{2}}\right]+|0\rangle\right\}.$$

Similarly, the high-K limiting behavior of the energy levels can be obtained by expanding the square root in Eq. (A8) as a power series in $1/\Delta$. To terms of lowest nonvanishing order in $1/\Delta$, the energy levels are given by

$$E_0=E_K+\epsilon'_\Pi,$$

$$E_-=E_K+\frac{\epsilon'_\Pi+\epsilon'_\Sigma}{2}-2BQ\sqrt{K(K+1)}-\frac{|\Delta\epsilon'|}{4}\frac{1}{\Delta}, \tag{A15}$$

$$E_+=E_K+\frac{\epsilon'_\Pi+\epsilon'_\Sigma}{2}+2BQ\sqrt{K(K+1)}+\frac{|\Delta\epsilon'|}{4}\frac{1}{\Delta},$$

and the associated wave functions by

$$\Psi_0^{E,K,M}=\left(\frac{-D^{K*}_{K,1}|1\rangle+D^{K*}_{K,-1}|-1\rangle}{\sqrt{2}}\right),$$

$$\Psi_-^{E,K,M}=\frac{i}{\sqrt{1+\left(1-\frac{1}{\Delta}\right)^2}}\left[\left(\frac{D^{K*}_{K,1}|1\rangle+D^{K*}_{K,-1}|-1\rangle}{\sqrt{2}}\right)+\left(1-\frac{1}{\Delta}\right)(D^{K*}_{K,0}|0\rangle)\right], \tag{A16}$$

$$\Psi_+^{E,K,M}=\frac{1}{\sqrt{1+\left(1-\frac{1}{\Delta}\right)^2}}\left[(D^{K*}_{K,0}|0\rangle)+\left(1-\frac{1}{\Delta}\right)\left(\frac{D^{K*}_{K,1}|1\rangle+D^{K*}_{K,-1}|-1\rangle}{\sqrt{2}}\right)\right].$$

Again, for the case of $M=K$, we use Eqs. (A3) and (A13) to rewrite these high-K limit wave functions in the equivalent form

$$\Psi_0^{E,K,M}=e^{iK\Phi}d^K_{K,0}(\Theta)\sqrt{\frac{K}{K+1}}\times\left[\frac{\cot\left(\frac{\Theta}{2}\right)|1\rangle-\tan\left(\frac{\Theta}{2}\right)|-1\rangle}{\sqrt{2}}\right],$$

$$\Psi_-^{E,K,M}=\frac{e^{iK\Phi}d^K_{K,0}(\Theta)}{\sqrt{1+\left(1-\frac{1}{\Delta}\right)^2}}\left\{\sqrt{\frac{K}{K+1}}\times\left[\frac{\cot\left(\frac{\Theta}{2}\right)|1\rangle+\tan\left(\frac{\Theta}{2}\right)|-1\rangle}{i\sqrt{2}}\right]+i\left(1-\frac{1}{\Delta}\right)|0\rangle\right\}, \tag{A17}$$

$$\Psi_+^{E,K,M}=\frac{e^{iK\Phi}d^K_{K,0}(\Theta)}{\sqrt{1+\left(1-\frac{1}{\Delta}\right)^2}}\left\{|0\rangle-i\left(1-\frac{1}{\Delta}\right)\sqrt{\frac{K}{K+1}}\times\left[\frac{\cot\left(\frac{\Theta}{2}\right)|1\rangle+\tan\left(\frac{\Theta}{2}\right)|-1\rangle}{i\sqrt{2}}\right]\right\}.$$

The above formulas for energy levels and wave functions are easy enough to derive, but it is hard to see their physical meaning. In Sec. III we compare these rigorous full quantum results with those of our more intuitive semiclassical treatment.

[1] J. H. Van Vleck, Phys. Rev. **33**, 467 (1929).
[2] R. S. Mulliken and A. Christy, Phy. Rev. **38**, 87 (1931).
[3] G. Herzberg, *Molecular Spectra and Molecular Structure I. Spectra of Diatomic Molecules* (Van Nostrand Reinhold, New York, 1950), pp. 212–231.
[4] J. T. Hougen, Natl. Bur. Stand. Monograph 115 (1970).
[5] R. N. Zare, A. L. Schmeltekopf, W. J. Harrop, and D. L. Albritton, J. Mol. Spectrosc. **46**, 37 (1973).
[6] H. Helm, R. P. Saxon, and D. L. Huestis, J. Chem. Phys. **76**, 2516 (1982).
[7] J. B. Norman and R. W. Field, J. Chem. Phys. **92**, 76 (1990).
[8] A. C. Luntz, A. W. Kleyn, and D. J. Auerbach, J. Chem. Phys. **76**, 737 (1982).
[9] P. Andresen and E. W. Rothe, J. Chem. Phys. **82**, 3634 (1985).
[10] P. W. Atkins, *Molecular Quantum Mechanics*, 2nd ed. (Oxford University Press, Oxford, 1983).
[11] L. J. Kovalenko, S. R. Leone, and J. B. Delos, J. Chem. Phys. **91**, 6948 (1989).
[12] We use the symbol **N** for nuclear angular momentum rather than the conventional symbol **R** so as not to confuse nuclear angular momentum with the nuclear trajectory, **R**.
[13] E. U. Condon and G. H. Shortley, *The Theory of Atomic Spectra* (Cambridge University Press, Cambridge, 1963).
[14] Through out this paper we consider the case where $\epsilon_\Sigma > \epsilon_\pi$. In the opposite case, the ϵ_Σ is replaced by ϵ_π and the ϵ_π by ϵ_Σ in Eq. (10).
[15] R. N. Zare, *Angular Momentum* (Wiley, New York, 1988).
[16] The following statement in Ref. 15 on p. 297: ''The choice of $\chi=0$ implies that the molecule-fixed Y axis coincides with the line of nodes, that is, lies in the plane of rotation, while the molecule-fixed X axis is perpendicular to the plane of rotation, which is the direction **J** points in the high J limit.'' can be confusing. This statement is true only for $|M| \cong K$. The body-fixed axis which is perpendicular to the plane of rotation depends on the choice of *both* M and χ. For a choice of $M=K$ and $\chi=0$, the X axis is perpendicular to the plane of rotation, while for $M=0$ and $\chi=0$ the Y axis is perpendicular to the plane of rotation.
[17] J. B. Delos, Rev. Mod. Phys. **53**, 287 (1981).
[18] The $\mathbf{L}^2$ operator is diagonal in this representation; it is shown in reference 4 that its matrix elements for $L=1$ are all equal.
[19] A. R. Edmonds, *Angular Momentum in Quantum Mechanics* (Princeton University Press, Princeton, 1974), where we have re-expressed the equation in terms of ''active'' d's of Zare.